Available online at www.sciencedirect.com

SciVerse ScienceDirect

Ceramics International 39 (2013) 4839–4846

CERAMICS INTERNATIONAL

www.elsevier.com/locate/ceramint

Influence of the calcination temperature on morphological and mechanical properties of highly porous hydroxyapatite scaffolds

Scalera F.*, Gervaso F., Sanosh K.P., Sannino A., Licciulli A.

Department of Engineering for Innovation, University of Salento, Lecce 73100, Italy

Received 12 October 2012; received in revised form 21 November 2012; accepted 23 November 2012
Available online 3 December 2012

Abstract

Bone tissue engineering is a promising approach for bone replacement or augmentation. However, the achievement of a high performing scaffold is still undergoing. In this work, the optimum calcination temperature value of the starting powder for the preparation of highly porous hydroxyapatite scaffold, fabricated by the sponge replica method, was assessed. Hydroxyapatite nanopowder was synthesized by the precipitation method and the influence of four calcinations temperatures (600, 700, 800 and 900 °C) on either powder characteristics or scaffold properties were exhaustively examined. Powder composition and grain size were determined by XRD, TEM and BET analyses. Composition, morphology, porosity, shrinkage and mechanical strength of the sintered scaffolds were determined by XRD, FT-IR, weight and dimension measurements and compression tests. The results showed that increasing the calcination temperature, the grain size of the HA powder increases and a higher grain size leads to a more resistant HA scaffold. The 900 °C calcinations temperature provide the best performing scaffold without inducing any phase transformation. The study here reported highlighted that the calcinations treatment is essential to fabricate high resistant HA scaffolds.

Keywords: B. Grain size; C. Mechanical properties; Calcination temperature; Hydroxyapatite scaffolds

1. Introduction

Nowadays the development of porous synthetic material as bone substitutes for the filling of both load-bearing and non-load-bearing application is much attracting in dentistry and medicine field [1–4]. Currently, when a bone injures and the damaged tissue requires repair, substitution or augmentation, the most adopted solutions is the use of autografts or allografts. Although both autografts and allografts present some undisputed advantages such as osteoinduction and osteogenity, they also have important drawbacks i.e. rejection or viral infection, high costs, scarce availability and trauma [5,6]. A synthetic scaffold could be a promising alternative to the current therapies [3–7].

As reported in literature, two key parameters for the obtainment of a successful synthetic bone substitute are both material and structure morphology [8].

Hydroxyapatite (HA), Ca_{10} $(PO_4)_6(OH)_2$, one of the most biocompatible ceramics, is a good candidate for the developing of promising synthetic scaffolds because its significant chemical and physical resemblance to the mineral constituents of human bones and teeth. It has excellent biocompatibility, bioactivity and osteoconductive properties [9–11].

Crucial factors influencing the processing of HA products are synthesis methods and properties of the starting powder. Among the numerous synthesis routes developed for the production of HA powder, the precipitation technique has been widely used [12]. It has been demonstrated [13] to allow the control of important powder parameters (such as, i.e., uniformity and nano grain size) and it is also a relatively simple and cheap process. Although, afterwards, in order to get a starting powder with suitable properties for high-quality sample forming and sintering, a heat treatment process, named calcination, is required to modify the raw nano-HA powder. Juang and Hon [14] studied the effects of calcination on the sintering behaviors of dense HA and found that the calcination not

*Corresponding author. Tel.: +39 349 8105933.
E-mail address: francesca.scalera@unisalento.it (F. Scalera).

0272-8842/$ - see front matter © 2012 Elsevier Ltd and Techna Group S.r.l. All rights reserved.
http://dx.doi.org/10.1016/j.ceramint.2012.11.076

only improves the properties of sintered HA, but it is also beneficial for several forming process like, for example, injection molding and slip casting because of a better packing of the ceramic grains and a more fluidity capability of the slurries.

A synthetic scaffold should resemble the natural bone not only in relation to the composition material but also to the structure morphology. A structure with a high and highly interconnected porosity should be hence mandatory for a synthetic bone substitute [15,16]. Due to its large surface area, porous scaffold simulates human bone structure for adhesion of biological tissue cell and growth of new bone phase [17,18]. The most common techniques that are used to create porosity in synthetic biomaterial include gel casting, slip casting, fiber compacting, solid free form fabrication, freeze casting and sponge replica method [19–28]. The most important feature of polymeric sponge method is that it makes possible the fabrication of scaffolds with required pore size and interconnected pores, which is necessary in order to allow cell migration, vascularization and nutrient diffusion [16,17].

The starting powder properties are all the more so important if not a dense sample but a highly porous ceramic scaffold has to be fabricated [29,30]. Hence, in order to get scaffolds with desired properties, the starting powder should have optimal surface area, particle size and crystalline phase. These parameters can be attained by proper calcination of the synthesized powder. Although the effect of temperature of calcination on the characteristics of a sol–gel synthesized HA powder and on the properties of dense HA samples has already been reported [12–14], at the best of our knowledge, the calcination temperature effect on morphological and mechanical properties of a highly porous HA scaffold has not been studied yet.

Therefore, aim of the present study is to investigate the relationship between the calcination temperature of a nano-HA powder prepared by the precipitation method and the properties of a highly porous scaffold prepared with the aforesaid powder. More in detail, the influence of the calcination temperature on the (i) grain size, (ii) surface area and (iii) composition of the HA powder synthesized by the precipitation method will be evaluated. Four different calcination temperatures will be analyzed (600, 700, 800 and 900 °C) and, with them, four typologies of scaffold (according to the powder used) fabricated by the sponge replica method. The changes in the sinterability, morphology and mechanical performance of the scaffolds prepared with the powder calcined at the four different temperatures will be assessed and presented.

2. Materials and methods

2.1. Synthesis and characterization of hydroxyapatite powders

The HA powder was synthesized from the co-precipitation of $Ca(NO_3)_2 4H_2O$ (Sigma Aldrich, Germany) and H_3PO_4 (Sigma Aldrich, Germany) at room temperature. The pH of the solution was maintained at 10 adding small amount of ammonia during the precipitation. The Ca/P ratio was kept 1.67 in order to get stoichiometric hydroxyapatite. After the precipitation the solution was aged in the water bath for 24 h. The precipitates were filtered and then dried at 100 °C for 24 h.

The obtained powder was divided in four groups that were calcined for 2 h each at one of the following calcination temperatures: 600, 700, 800 and 900 °C. The powders were named HA600, HA700, HA800, and HA900 respectively. The morphology and the particle size of the powder before and after calcination were evaluated by transmission electron microscope (TEM) analysis (HRTEM, Model Tecnai-Philips F30, FEI, Hillsboro, OR).

The influence of calcination temperature on powders composition, crystallinity and grain size was analyzed by powder X-ray diffraction (Rigaku, Tokyo, Japan). Phases were identified by comparing X-ray diffractograms taken from the experiment to standards complied by the Joint Committee on Powder Diffraction Standards (JCPDS) using the cards 09-0432 for HA.

The fraction of crystalline phase χ_c present in the HA powders was evaluated by the relation [31]

$$\chi_c = 1 - \left(\left(v_{112/300} \right) / I_{300} \right) \quad (1)$$

where I_{300} is the intensity of (300) reflection and $V_{112/300}$ is the intensity of the hollow between (112) and (300) reflections.

Coherent domain sizes (D) of all four powders were estimated according to Scherrer's equation

$$D = (0.9\lambda)/(B_{½} \cos q) \quad (2)$$

where λ is the wavelength of the x-ray (nm), $B_{1/2}$ is the full width at the half maximum peak intensity, θ is the Bragg diffraction.

The specific surface area (SS) of the powders was calculated by the Brunauer–Emmett–Teller method with nitrogen as the adsorbate gas (Nova 2200e from Quantachrome Instruments (Boynton Beach, FL)). The size of the crystallites was estimated from BET surface area by calculating the equivalent spherical diameter, d_{BET}, from the following equation:

$$d_{BET} = 6/\rho SS \quad (3)$$

where ρ is the density of the powder. A density of 3.156 g/cm^3, which is the theoretical density of stoichiometric HA, was used.

2.2. Fabrication and characterization of the porous HA scaffolds

To mimic the bone structure, that shows a high degree of porosity interconnection, the sponge replica method was used. Cubic sponges (dimensions of $10 \times 10 \times 10$ mm^3, density of 30 kg/m^3, 25 ppi, kindly provided by ORSA Foam S.p.A.) were impregnated with four different

slurries, prepared with each powder, then well squeezed. The slurries (with approximately 70 wt% of solid load) were prepared using the following procedure: the calcined powders were dispersed in a 2 wt% of PVA solution. Dolapix (Dolapix CE-64, Zschimmer–Scwarz, Lahnstein, Germany) was used as dispersant to obtain an adequate viscosity of slurries for the impregnation. Before the sintering they were dried at room temperature for 24 h.

At last, the infiltrated sponges were heated to 500 °C at a heating velocity of 1 °C/min and held at 500 °C for 1 h in order to assure the burnout process of the foam was completed; afterwards, the samples were sintered at 1300 °C for 3 h then slowly cooled till room temperature. The scaffolds were named S-HA600, S-HA700, S-HA800, and S-HA900 according to the starting powder.

The purity and the crystallinity of HA scaffolds sintered till 1300 °C was evaluated by XRD analysis and the presence of functional groups was also analyzed by FTIR (Agilent 680-IR) within the scanning range of 4000–600 cm^{-1}.

Micrographs at 60× and 2000×, taken using a scanning electron microscope (SEM; Philips XL30), were used to characterize the macroscopic and microscopic morphology of the sintered foams. A caliper was used to measure the linear shrinkage (δ) of scaffold as

$$\delta = 1 - l/l_0 \quad (4)$$

where l_0 is the length of the green and l is the length of the sintered body.

The porosity of the ceramic foams was then calculated using the following:

$$P = 1 - \rho/\rho_{HA} \quad (5)$$

where ρ is the bulk density of sintered specimens and ρ_{HA} is the theoretical density of the pure HA (3.156 g/cm^3).

The mechanical properties of the scaffolds were evaluated by compression tests. The tests were performed using a standard testing machine (Lloyd LR5K instrument, Fareham Hants, UK) equipped with a 1 kN load cell. The cubic scaffolds were tested under compression and the compressive stress was calculated from applied load and cross sectional area of the cube ($\sigma = P/A$) and plotted as function of the strain.

The stress at failure (σ_F) (maximum fracture load/cross-sectional area) and the Young Modulus E (slope of the linear region of the stress–strain curve) were calculated for each samples.

3. Results

3.1. Physical properties and composition of hydroxyapatite powders

To investigate the influence of the calcination temperature on the sinterability and mechanical properties of the HA scaffolds, four types of powders were prepared and characterized. The morphology and size of the HA powder before and after heat treatment are shown in Fig. 1 where TEM images are reported. The HA particles both before and after calcination looks agglomerate, the uncalcined powder showa particle size of in the range of 30–40 nm while the 900 °C calcined increases to150–200 nm. The XRD patterns of the four powders are shown in Fig. 2.The spectra of all powders (HA600, HA700, HA800 and HA900) show the diffraction maxima corresponding to a pure HA phase (JCPDS 09-0432) without any secondary phase.The intensity of the defractionpeaks increases with calcination temperature while the peaks becomes narrower

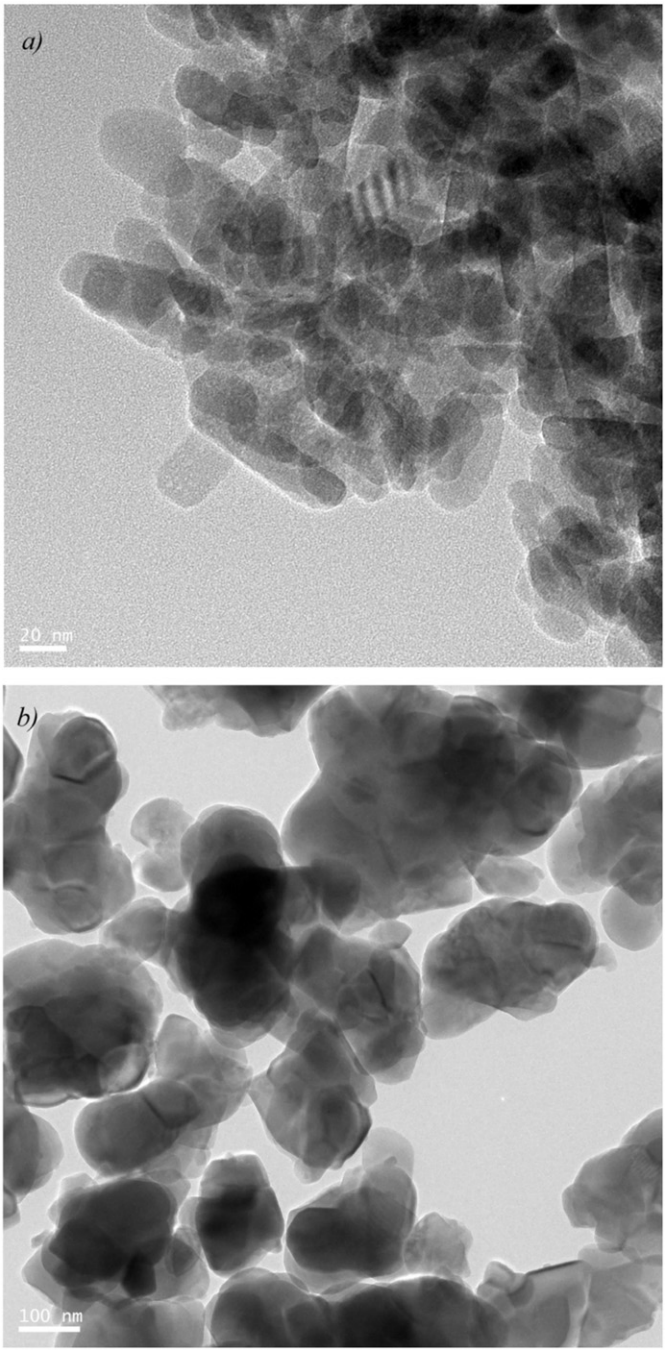

Fig. 1. TEM images of the HA powder before (a) and after (b) the 900 °C calcination treatment.

indicating an increasing of the crystallinity because of the higher coalescence of the hydroxyapatite crystals. The crystalinity was calculated according to formulae (1) and the values are reported in Table 1 as a function of the calcination temperature. The crystallinity of HA powder reaches 52% when a calcination at 600 °C was performed and increases up to 87% when temperature reaches 900 °C.

The size of crystals was calculated according to Scherrer formula and the average values are reported in Table 1. Increasing the calcination temperature from 600 °C to 900 °C the crystal size increases linearly from 17 nm to 37 nm.

In Table 1, the specific surface area of the four HA powders is also reported. The SS of the powders decreases increasing the calcination temperature (from 38 for the HA600 to 9 m^2/g for the HA900) as a consequence of the equivalent grain diameter increase (from 52 nm to 220 nm).

3.2. Scaffold morphology, microstructure and composition

In Fig. 3(a) and (b) the XRD and FT-IR spectra of HA scaffold are shown. From XRD analysis it is clear that (i) the powder is thermally stable till 1300 °C, (ii) no secondary phases form and (iii) the crystallinity reaches 94%. From the FTIR spectrum, the absorption bands at wave numbers 1090, 1027 and 960 cm^{-1} are associated with the characteristic of PO_4^{-3} group, whereas, band at 3572 cm^{-1} shows the characteristic stretching mode for OH^- group[32]. Thus, the FTIR analysis indicates the sintered scaffold is free from other impurities.

Fig. 4 shows the macrostructureof the four types of scaffolds S-HA600 (a), S-HA700 (b), S-HA800 (c) and S-HA900 (d). The four ceramic sponges exhibit a highly interconnected porous structure with open poreshaving an average size of 400–500 μm. From the SEM images reported in Fig. 4(a)–(c) ,it is possible to detect also the presence of micro-voids of sub-micron scale (secondary

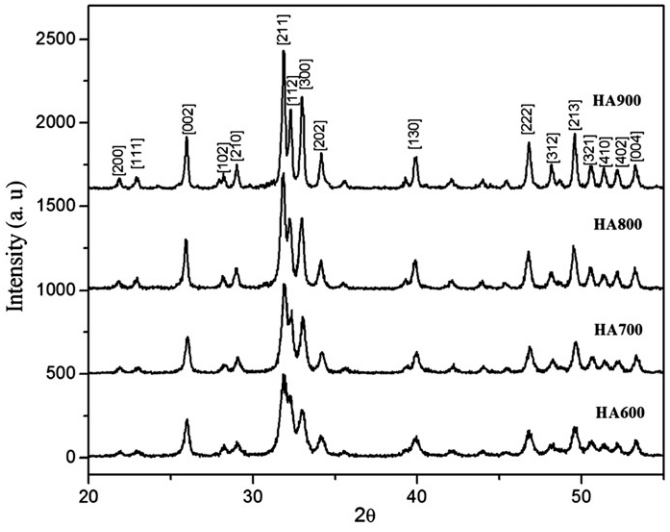

Fig. 2. XRD spectra of the HA powders at the four calcination temperatures (600, 700, 800 and 900 °C).

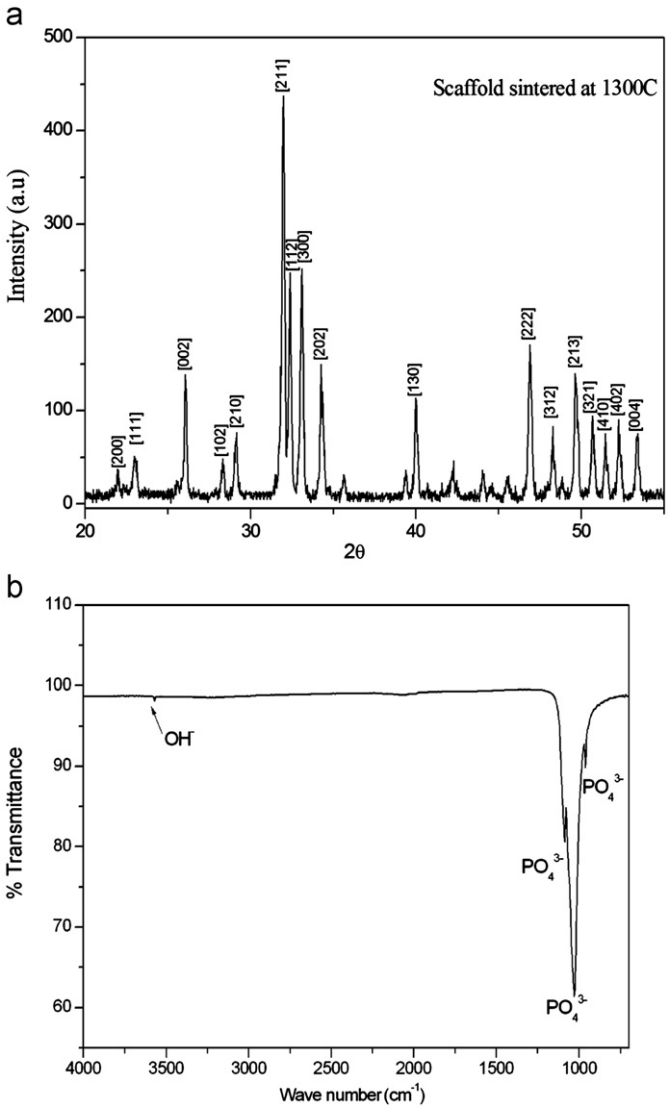

Fig. 3. XRD (a) and FTIR (b) spectra of the HA scaffold sintered at 1300 °C.

Table 1
HA powder characteristics as a function of the calcination temperature.

Calcination temperature (°C)	χ_c (%)	Crystal size (nm)	Specific surface area (m^2/g)	Equivalent diameter (nm)
600	52 ± 4	17 ± 3	38	52
700	67 ± 3	21 ± 4	26	77
800	79 ± 3	27 ± 4	15	135
900	87 ± 2	37 ± 3	9	220

porosity, indicated by arrows). Instead, in the scaffolds made with powder HA900 (Fig. 4d), the presence of the micro-voids is significantly reduced. From the SEM observation performed on the four scaffolds at higher magnification, the strut surface of the S-HA600, S-HA700 and S-HA800 scaffolds (Fig. 5(a)–(c)) appears not

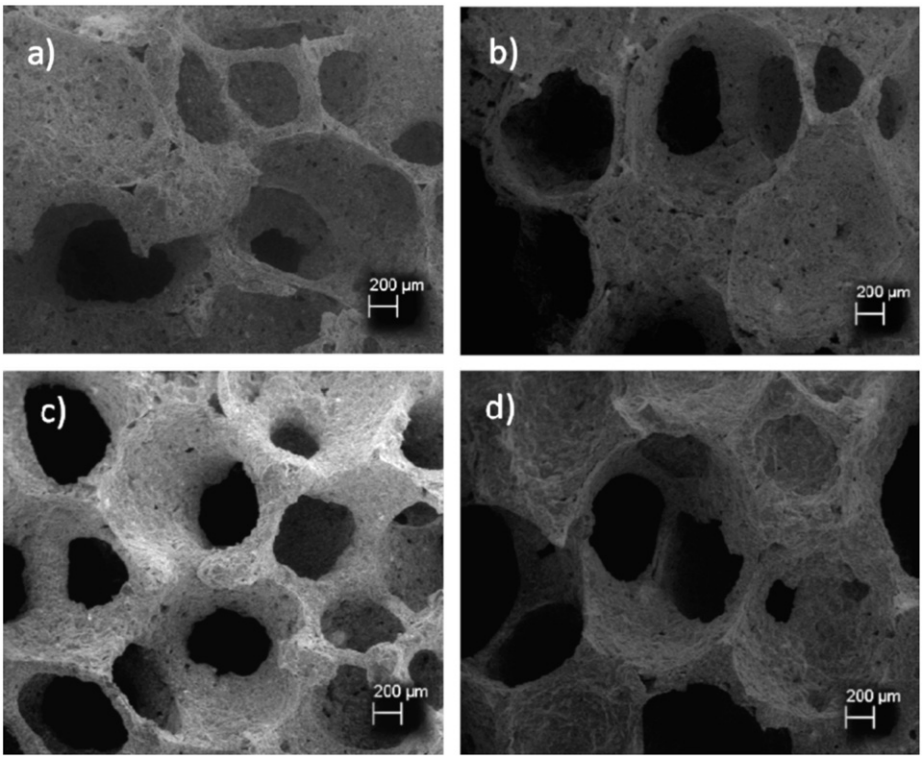

Fig. 4. SEM images of scaffolds S-HA600 (a), S-HA700 (b), S-HA800 (c) and S-HA900 (d) at 60 × .

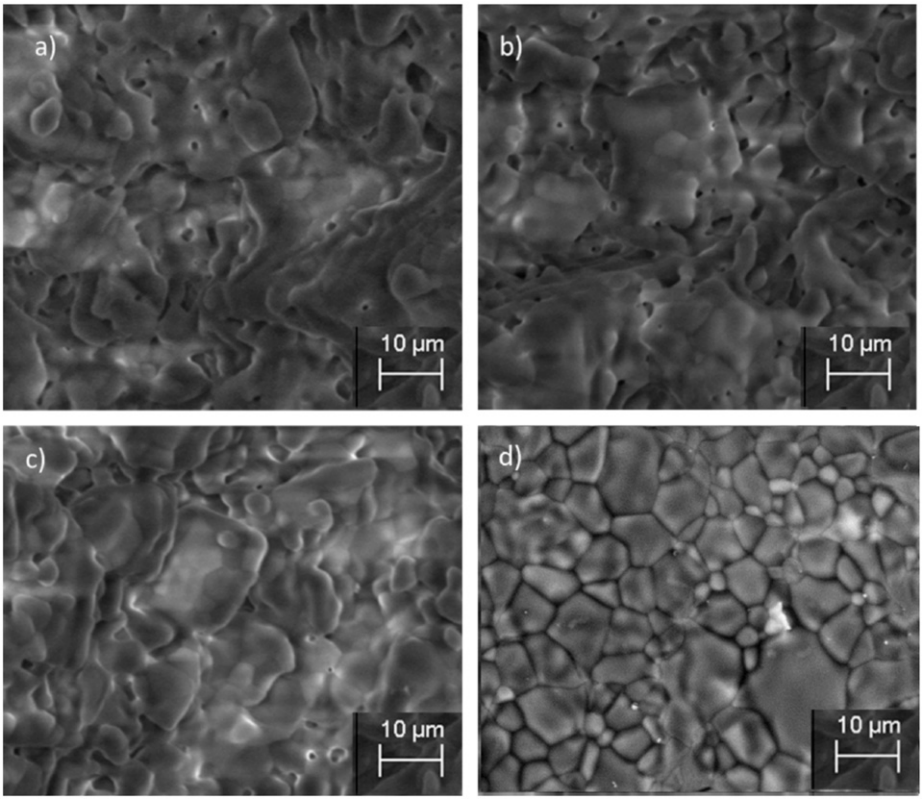

Fig. 5. SEM images of scaffolds S-HA600 (a), S-HA700 (b), S-HA800 (c) and S-HA900 (d) at 2000 × .

Table 2
HA scaffold shrinkage, density and porosity as a function of the calcination temperature.

Calcination temperature (°C)	Linear shrinkage (δ) (%)	Bulk density (ρ) (g/cm^3)	Porosity (P) (%)
600	16.9 ± 3.4	0.67 ± 0.03	79 ± 1
700	20.5 ± 1.4	0.29 ± 0.08	91 ± 3
800	20.7 ± 0.1	0.29 ± 0.07	91 ± 2
900	25.6 ± 2.5	0.34 ± 0.06	89 ± 2

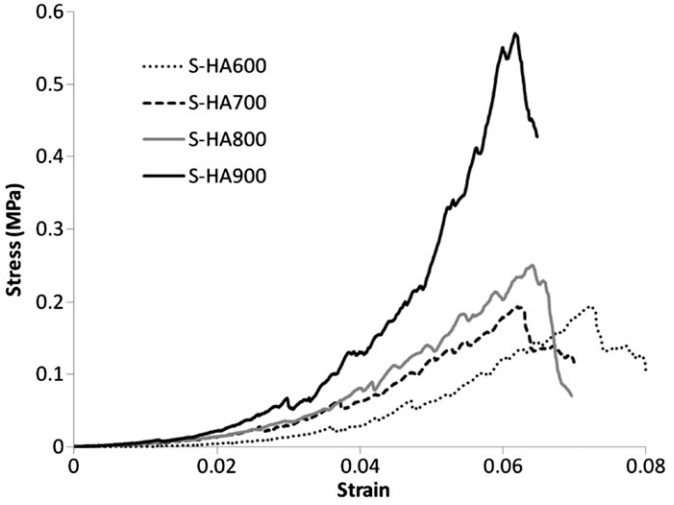

Fig. 6. Stress–strain curves obtained by the compression test performed on samples fabricated with the four powder calcined at the four analyzed temperatures: S-HA600, S-HA700, S-HA800 and S-HA900.

perfectly smooth with ceramic grains variable in shape and in size (between 2 and 8 μm). The micro-voids detected in Fig. 4 are also visible here and show a submicron size (indicated by arrows). On the contrary, the microstructure of the scaffold S-HA900 appears very different with respect to the other scaffolds, the micro-voids are absent and the grain size well distinguishable with defined boundaries (Fig. 5(d)).

3.3. Scaffold shrinkage, porosity and compressive strength

In Table 2 are summarized the linear shrinkage, the bulk density and the porosity percentages of the four types of scaffolds prepared with the different powders. It can be noticed that, increasing the calcination temperature, the linear shrinkage increases from 17% to 26%. The porosity is almost 90% for all scaffolds except for those prepared with the powder calcined at 600 °C that presented a lower porosity value of 78%.

Fig. 6 shows the stress–strain curves for the scaffolds synthesized from all the ceramic powders calcined at 600, 700, 800 and 900 °C. The curves show the typical trend of ceramic materials subjected to compression test: after an initial compaction phase, the slope changes and the stress increases linearly up to failure. In Table 3 the average and

Table 3
Mechanical properties of the HA scaffold as a function of the calcination temperature.

Calcination temperature (°C)	Failure stress (σ_F) (MPa)	Young modulus (MPa)
600	0.18 ± 0.10	1.08 ± 1.09
700	0.17 ± 0.08	4.76 ± 0.43
800	0.20 ± 0.06	7.34 ± 1.88
900	0.48 ± 0.08	28.09 ± 9.3

the standard deviations of failure stress (maximum stress) and Young modulus values are reported for S-HA600, S-HA700, S-HA800 and S-HA900 scaffolds. According to linear shrinkage behavior, stress at failure increases increasing the calcination temperature. The S-HA900 scaffolds showed the superior mechanical properties with a maximum stress value equal to 0.48 MPa and a Young modulus of about 28 MPa.

4. Discussion

The precipitation method used in this study allowed the synthesis of a pure nano-HA. The XRD analysis showed that no secondary phases are present either in the uncalcined or in the calcined powders. The thermal stability of the HA powder at high temperatures such as 900 °C depends on the initial ratio of the precursors (i.e. Ca/P) and also on the synthesis route employed for HA production as already reported by Sanosh KP et al. [33,34].

The TEM analysis showed that the grain size of the uncalcined powder increases from 30 nm to 200 nm increasing the calcinations temperature to 900 °C. These results are well accordance with the grain size obtained from specific surface area measurement by the BET method that provided an equivalent diameter of 220 nm for the HA900.

The powders obtained according to the four calcination temperatures were successfully used to get scaffolds with a high porosity (90%) with well interconnected pores. The porosity and the interconnection of the macropores in a bone substitute are considered essential for the ingrowth of the bone tissue and a pore size greater than 300 μm is desirable in order to promote osteogenesis [35]. All the scaffolds fabricated in the present study own the morphological requirements to perform the function they are

designed for, as indicated by SEM images (Figs. 4 and 5) that show a high interconnection and a pore size of about 500 μm. However, the S-HA600 presented porosity significantly lower than the others. In this case, the slurry did not present the suitable viscosity, therefore, in order to get a uniform impregnation of the polymeric sponge, a bigger amount of ceramic slurry had to be used, causing a significant increase in the bulk density of the scaffold and hence a substantial decrease of the porosity.

The mechanical characterization evidenced that the S-HA900 are the most performing scaffolds, showing a compression resistance of about 0.5 MPa higher [36,37] or significantly higher [38,39] than mechanical resistance reported by other authors. Moreover, the mechanical results obtained with the calcination temperature of 900 °C has been validated by a statistical model reported in a previous study of the same authors [40].

Decreasing the calcinations temperature, the mechanical strength decreases significantly while the shrinkage decreases. This should be a result of an imperfect sintering probably due to a bad coarsening of the powders. In fact, the calcination at a high temperature (few hundred below the sintering temperature) makes the ceramic powder more reactive inducing during the sintering phase higher grain coalescence and consequently an increase of the linear shrinkage. More in detail, finer HA powder at low calcination temperatures provides more surface as driving force of sintering but, at the same time, Van der Waal force becomes more significant, retarding the packing of HA powder. Therefore, the calcination increases the efficiency of powder packing, though driving force is sacrificed in the mean time. In this study, calcination treatment at 900 °C results beneficial on the sintered scaffolds properties because leads to the best compromise between the two effects described above.

5. Conclusions

The present study demonstrated that (i) the calcination treatment performed on HA powder synthesized by precipitation method did not induce any phases transformation; (ii) a reduction of surface area and an increase in the grain size was obtained by increasing the calcination temperature from 600 °C to 900 °C; (iii) the composition of the scaffold obtained by the polymeric sponge method using the powder calcined at the four analyzed temperatures was not affect by the sintering temperature of 1300 °C (iv) the optimal scaffolds with the highest mechanical strength were obtained when starting powder underwent calcination treatment at 900 °C and (v) the key factor governing the sintering mechanism could be that the calcination increases the efficiency of powder packing more than the driving force due to surface area.

We can conclude that the calcination treatment is a mandatory step for producing high performing scaffold for the bone tissue-engineering application.

References

[1] P.K. Bajpai, Biodegradable scaffolds in orthopedic, oral and maxillofacial surgery, in: L.R. Rubin (Ed.), Biomaterials in Reconstructive Surgery, St. Louis Mosby, St. Louis (MO), 1983, p. 156.
[2] J.O. Hollinger, A. Chaudhari, Bone regeneration materials for the mandibular and craniofacial complex, Cells and Materials 2 (1992) 143–151.
[3] R.G. Kavanagh, J.S. Butler, J.M. O'Byrne, A.R. Poynton, Operative techniques for cervical radiculopathy and myelopathy, Advances in Orthopedics (2012) 794087.
[4] O. Faour, R. Dimitriou, C.A. Cousins, P.V. Giannoudis, The use of bone graft substitutes in large cancellous voids: any specific needs?, Injury 42 (2011) 87–90
[5] G.M. Calori, E. Mazza, M. Colombo, C. Ripamonti, The use of bone-graft substitutes in large bone defects: any specific needs?, Injury 42 (2011) 56–63
[6] S.W. Laurie, L.B. Kaban, J.B. Mulliken, J.E. Murray, Donor-site morbidity after harvesting rib and iliac bone, Plastic and Reconstructive Surgery 73 (1984) 933–938.
[7] A. Kolk, J. Handschel, W. Drescher, D. Rothamel, F. Kloss, M. Blessmann, M. Heiland, K.D. Wolff, R.J. Smeets, Current trends and future perspectives of bone substitute materails-from space holders to innovative biomaterials, Journal of Cranio-Maxillofacial Surgery (2012).
[8] P. Petrochenko, R.J. Narayan, Novel approaches to bone grafting: porosity, bone morphogenetic proteins, stem cells, and the periosteum, Journal of Long Term Effects of Medical Implants 20 (2010) 303–315 (Review).
[9] L.L. Hench, Bioceramics, from concept to clinic, Journal of the American Ceramic Society 74 (1991) 1487–1510.
[10] G. Bonel, Hydroxyapatite biomaterials: industrial and clinical aspects; evolution of the conception, in: E. Bres, P. Hardouin (Eds.), Calcium Phosphate Materials Fundamentals, Sauramps Medical, Montpellier, France, 1998, pp. 9–24.
[11] R.W. Bucholz, A. Carlton, R.E. Holmes, Hydroxyapatite and tricalcium phosphate bone graft substitutes, The Orthopedic Clinics of North America 18 (1987) 323–334.
[12] K. Seema, B. Uma, K. Suchita, Transformations in sol–gel synthesized nanoscale hydroxyapatite calcined under different temperatures and time conditions, Journal of Materials Engineering and Performance 21 (2012) 1737–1743.
[13] K.P. Sanosh, M.C. Chu, A. Balakrishnan, T.N. Kim, S.J. Cho, Preparation and characterization of nano-hydroxyapatite powder using the sol–gel technique, Bulletin of Materials Science 32 (2009) 465–470.
[14] H.Y. Juang, M.H. Hon, Effect of calcination on sintering of hydroxyapatite, Biomaterials 17 (1996) 2059–2064.
[15] H. Yoshikawa, A. Myoui, Bone tissue engineering with porous hydroxyapatite ceramics, Journal of Artificial Organs 8 (2005) 131–136.
[16] H. Yoshikawa, N. Tamai, T. Murase, A. Myoui, Interconnected porous hydroxy-apatite ceramics for bone tissue engineering, Journal of the Royal Society Interface 6 (2009) 341–348.
[17] S. Yang, K.F. Leong, Z. Du, C.K. Chua, The design of scaffolds for use in tissue engineering Part I traditional factors, Tissue Engineering 7 (2001) 679–689.
[18] N. Tamai, A. Myoui, T. Tomita, T. Nakase, J. Tanaka, T. Ochi, H. Yoshikawa, Novel hydroxyapatite ceramics with an interconnective porous structure exhibit superior osteoconduction in vivo, Journal of Biomedical Materials Research 59 (2002) 110–117.
[19] P. Sepulveda, F.S. Ortega, M.D.M. Innocentini, V.C. Pandolfelli, Properties of highly porous hydroxyapatite obtained by the gelcasting of foams, Journal of the American Ceramic Society 83 (2000) 3021–3024.
[20] J.R. Woodard, A.J. Hilldore, S.K. Lan, C.J. Park, A.W. Morgan, J.A. Eurell, S.G. Clark, M.B. Wheeler, R.D. Jamison, A.J. Wagoner

Johnson, The mechanical properties and osteoconductivity of hydroxyapatite bone scaffolds with multi-scale porosity, Biomaterials 28 (2007) 45–54.
[21] L.D. Harris, B.S. Kim, D.J. Mooney, Open pore biodegradable matrices formed with gas foaming, Journal of Biomedical Materials Research 42 (1998) 396–402.
[22] L.A. Cyster, D.M. Grant, S.M. Howdle, F.R. Rose, D.J. Irvine, D. Freeman, C.A. Scotchford, K.M. Shakesheff, The influence of dispersant concentration on the pore morphology of hydroxyapatite ceramics for bone tissue engineering, Biomaterials 26 (2005) 697–702.
[23] Q. Fu, M.N. Rahaman, B.S. Bal, W. Huang, D.E. Day, Preparation and bioactive characteristics of a porous 13–93 glass, and its fabrication into the articulating surface of a proximal tibia, Journal of Biomedical Materials Research 82A (2007) 222–229.
[24] B.S. Chang, C.K. Lee, K.S. Hong, H.J. Youn, H.S. Ryu, S.S. Chung, K.W. Park, Osteoconduction at porous hydroxyapatite with various pore configurations, Biomaterials 21 (2000) 1291–1298.
[25] T.M. Chu, D.G. Orton, S.J. Hollister, S.E. Feinberg, J.W. Halloran, Mechanical and in vivo performance of hydroxyapatite implants with controlled architectures, Biomaterials 23 (2002) 1283–1293.
[26] Q. Fu, M.N. Rahaman, F. Dogan, B.S. Bal, Freeze casting of porous hydroxyapatite scaffolds. I. Processing and general microstructure, Journal of Biomedical Materials Research Part B: Applied Biomaterials 86 (2008) 125–135.
[27] A.C. Queiroz, S. Teixeira, J.D. Santos, F.J. Monteiro, Production of porous hydroxyapatite with potential for controlled drug delivery, Materials Science Forum 445 (2004) 358–360.
[28] A.C. Queiroz, S. Teixeira, J.D. Santos, F.J. Monteiro, Porous hydroxyapatite and glass reinforced hydroxyapatite for controlled release of sodium ampicillin, Key Engineering Materials 254–256 (2004) 997–1000.
[29] I.O. Smith, L.R. McCabe, M.J. Baumann, MC3T3-E1 osteoblast attachment and proliferation on porous hydroxyapatite scaffolds fabricated with nanophase powder, International Journal of Nanomedicine 1 (2006) 189–194.
[30] Q. Chen, D. Mohn, W.J. Stark, Optimization of bioglass scaffold fabrication process, Journal of the American Ceramic Society 94 (2011) 4184–4190.
[31] E. Landi, A. Tampieri, G. Celotti, S. Sprio, Densification behaviour and mechanisms of synthetic hydroxyapatites, Journal of The European Ceramic Society 20 (2000) 2377–2387.
[32] A. Slosarczyk, C. Paluszkiewicz, M. Gawlicki, Z. Paszkiewicz, The FTIR spectroscopy and QXRD studies of calcium phosphate based materials produced from the powder precursors with different Ca/P ratios, Ceramics International 23 (1997) 297–304.
[33] K.P. Sanosh, Min-Cheol Chu, A. Balakrishnan, T.N. Kim, Seong-Jai Cho, Pressureless sintering of nanocrystalline hydroxyapatite at different temperatures, Metals and Materials 16 (2010) 605–611.
[34] K.P. Sanosh, M.C. Chu, A. Balakrishnan, T.N. Kim, S.J. Cho, Sol–gel synthesis of pure nano sized beta-tricalcium phosphate crystalline powders, Current Applied Physics 10 (2010) 68–71.
[35] V. Karageorgiou, D. Kaplan, Porous of 3D biomaterials scaffolds and osteogenesis, Biomaterials 26 (2005) 5474–5491.
[36] S.I. Roohani-Esfahani, S. Nouri-Khorasani, Z. Lu, R. Appleyard, H. Zreiqat, The influence hydroxyapatite nanoparticle shape and size on the properties of biphasic calcium phosphate scaffolds coated with hydroxyapatite-PCL composites, Biomaterials 31 (2010) 5498–5509.
[37] J. Zhao, S. Xiao, X. Lu, J. Wang, J. Weng, A study on improving mechanical properties of porous HA tissue engineering scaffolds by hot isostatic pressing, Biomedical Materials 1 (2006) 188–192.
[38] X. Miao, D.M. Tan, J. Li, Y. Xiao, R. Crawford, Mechanical and biological properties of hydroxyapatite/tricalcium phosphate scaffolds coated with poly (lactic-co-glycolic acid), Acta Biomaterialia 4 (2008) 638–645.
[39] S. Teixeiraa, M.A. Rodriguezc, P. Penac, A.H. De Azac, S. De Azac, M.P. Ferraza, F.J. Monteiroa, Physical characterization of hydroxyapatite porous scaffolds for tissue engineering, Materials Science and Engineering C 29 (2009) 1510–1514.
[40] F. Gervaso, F. Scalera, SKunjalukkal Padmanabhan, A. Sannino, A. Licciulli, High-performance hydroxyapatite scaffolds for bone tissue engineering applications, International Journal of Applied Ceramic Technology 9 (2012) 507–516.